Lab on a Chip

PAPER

View Article Online
View Journal | View Issue

Cite this: *Lab Chip*, 2025, **25**, 2291

Dual lateral flow assay using quantum nanobeads for quantitative detection of BDNF and TNF-α in tears†

Yue Wu,[ab] Yubing Hu,[a] Nan Jiang,[c] Maria W. Georgi,[b] Ali K. Yetisen*[a] and M. Francesca Cordeiro*[bde]

Glaucoma is a group of neurodegenerative eye diseases characterized by progressive damage to the optic nerve which is typically asymptomatic until irreversible vision loss has occurred. Early screening is essential for timely treatment to prevent visual impairment. However, existing detection methods struggle to achieve a balance between accuracy, time efficiency, and portability. The lateral flow assay (LFA) is a well-established immunoanalytical tool for point-of-care (POC) analysis. Here, we have developed a unique dual-testing, quantum nanobeads-based fluorescence LFA, allowing for the simultaneous and quantitative detection of two glaucoma biomarkers: tumor necrosis factor-α (TNF-α) and brain-derived neurotrophic factor (BDNF). By coating quantum dots on the surface of a SiO_2 core, the fluorescent intensity of the quantum nanobeads was enhanced enabling an accurate, efficient, and high-throughput bioanalytical performance, with low detection limits of 3.39 pg mL^{-1} for TNF-α and 4.13 pg mL^{-1} for BDNF. The LFA also demonstrated superior selectivity, reproducibility, and stability to the standard enzyme-linked immunosorbent assay (ELISA). Using a 3D-printed readout box, the analysis of the LFA requires only a readily accessible smartphone and image processing software, making it an ideal POC detection tool. This ultrasensitive, economical, and user-friendly LFA demonstrates significant potential as an alternative for glaucoma screening.

Received 9th December 2024,
Accepted 2nd April 2025

DOI: 10.1039/d4lc01045k

rsc.li/loc

Introduction

Glaucoma is recognized as one of the leading causes of blindness worldwide,[1] often developing asymptomatically and leading to irreversible visual field defects in its advanced stages due to the chronic and progressive death of retinal ganglion cells.[2] Undiagnosed glaucoma rates are high, estimated at 70% in developed countries and even higher in developing regions.[3] The disease imposes both direct treatment and significant indirect costs, including $50 billion in expenses from associated falls and fractures in the United States alone.[4] Effective screening methods for early detection of glaucoma are crucial to prevent structural damage, reduce vision loss and minimize expenditures.[5]

Current diagnostic methods for glaucoma include intraocular pressure measurement, visual field testing and optic nerve examination. Whilst these methods are widely used, they fail to meet the stringent criteria for sensitivity and specificity required for a screening tool.[3,5,6] For instance, studies have shown that visual field tests demonstrated high false positive rate in mass screening.[7] Furthermore, the inter-physician variability of optic nerve assessment with ophthalmoscopy and fundus photography significantly affects result accuracy.[8] These limitations highlight the need for a more reliable, cost-effective, and user-friendly tool for glaucoma screening.

Recent advances in biomarker research have opened new avenues for non-invasive glaucoma detection. Tear fluid, in particular, has emerged as a valuable biomarker source.[9] Brain-derived neurotrophic factor (BDNF) and tumor necrosis factor alpha (TNF-α) are two such biomarkers which have demonstrated significant potential for early glaucoma detection. BDNF plays a vital role in the development and maintenance of the central nerve system.[10] Optic nerve damage in glaucoma patients disrupts the retrograde transport of BDNF, leading to axonal dystrophy and further

[a] *Department of Chemical Engineering, Imperial College London, South Kensington, London, UK. E-mail: a.yetisen@imperial.ac.uk*
[b] *Department of Surgery and Cancer, Imperial College London, South Kensington, London, UK. E-mail: m.cordeiro@imperial.ac.uk*
[c] *West China School of Basic Medical Sciences & Forensic Medicine, Sichuan University, Chengdu 610041, China*
[d] *The Imperial College Ophthalmic Research Group (ICORG), Imperial College London, London, UK*
[e] *Glaucoma and Retinal Neurodegeneration Group, Department of Visual Neuroscience, UCL Institute of Ophthalmology, London, UK*

† Electronic supplementary information (ESI) available. See DOI: https://doi.org/10.1039/d4lc01045k

injury the optic nerve.[11] Studies have reported significantly lower levels of BDNF in tear fluid of glaucoma patients (78.0 ± 25.1 pg mL^{-1} compared to 116.2 ± 43.1 pg mL^{-1} in control subjects) (Table S1†), particularly in the early stages of glaucoma (56.8 ± 10.3 pg mL^{-1}).[12] Cytokines, such as TNF-α, are also heavily involved in the pathophysiology of glaucoma, particularly in the loss of retinal ganglion cells.[13] TNF-α is a pro-inflammatory cytokine which plays various roles in the optic nerve system through different receptors:[13] through TNF-receptor 2 (TNF-R2), TNF-α exerts a neuroprotective action *via* the PI3K pathway;[14] however, activation of TNF-receptor 1 (TNF-R1) induces oxidative stress and inflammation, leading to neurodegenerationn.[13–15] Several studies have demonstrated elevated levels of TNF-α levels in tears, aqueous humor, and blood of glaucoma patients[16–19] (Table S1†). These findings highlight the significant potential of BDNF and TNF-α as dual biomarkers for the early detection of glaucoma.

Lateral flow assays (LFAs) represent a promising platform for point-of-care (POC) diagnostics due to their rapid, user-friendly, and cost-effective nature. LFAs have been widely used across various disciplines, including food safety,[20] environmental monitoring[21] and disease diagnosis.[22] Compared to other standard protein detection technologies such as enzyme-linked immunosorbent assays (ELISA), LFAs offer significant advantages in terms of speed, ease of use, and reduced dependence on sophisticated instruments and trained technicians,[23] suggesting high suitability for POC diagnosis. Furthermore, the sensitivity of LFA has been significantly enhanced due to the development of various novel labels that generate signals through mechanisms other than traditional

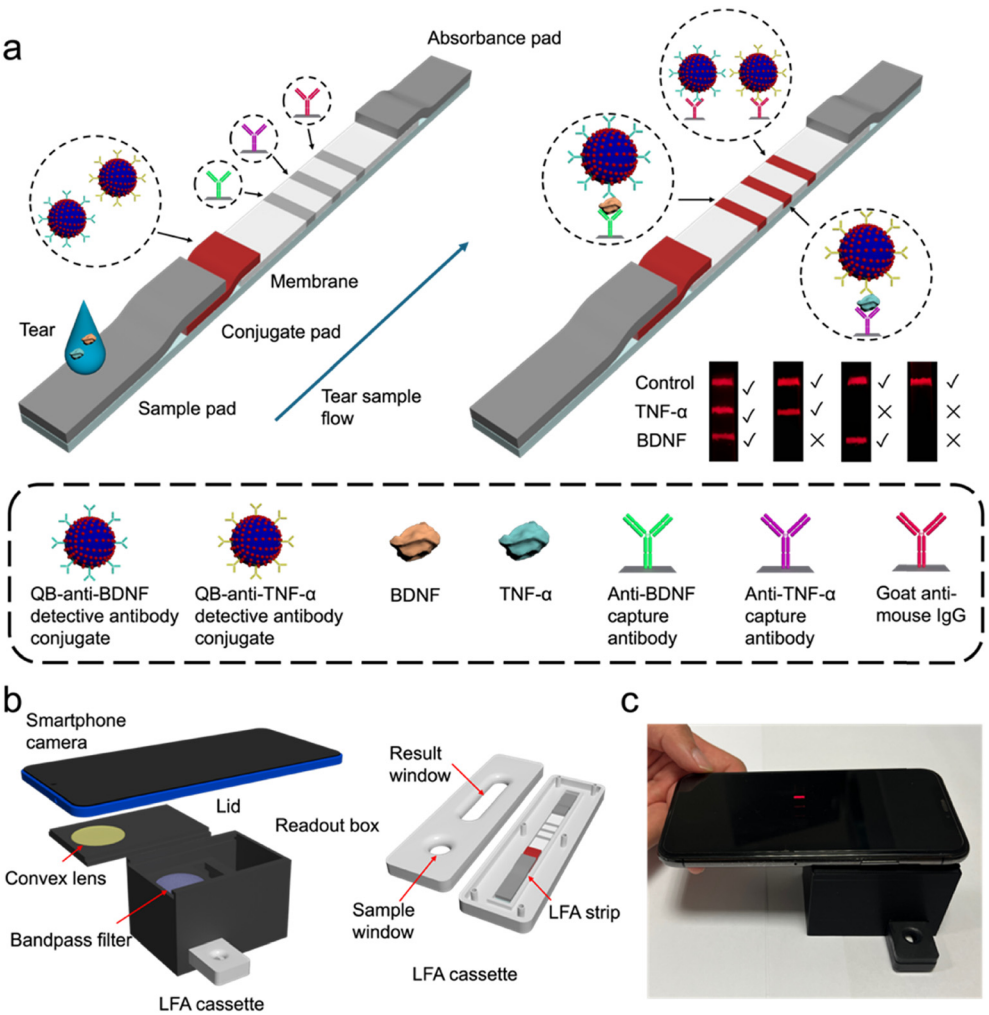

Fig. 1 Scheme of the dual-test LFA and readout system. a. The LFA strip consisted of sample pad, conjugate pad, membrane, and absorbance pad. The conjugate pad was impregnated with QB-labeled mouse sourced anti-human BDNF antibodies and anti-human TNF-α antibodies. The capture antibodies for human BDNF and TNF-α were fixed at the membrane as two test lines to capture the mixture of analyte and QB-labeled detective antibodies. The goat anti-mouse IgG specific to mouse sourced anti-human BDNF antibody and anti-human TNF-α antibody was printed in the membrane as the control line. b. The schematic illustration of the readout system. The readout system consists of a 3D printed box and integrated LED light, bandpass filter, and convex lens. The image of fluorescent LFA strips is captured by the smartphone camera and analyzed by ImageJ. c. Real image of readout system.

colorimetric methods.[24] For instance, fluorescence-based LFAs, particularly those utilizing quantum dots (QDs), have attracted increasing attention due to their superior analytical performance. QDs are notable for their narrow emission spectrum, wide excitation range, and high levels of brightness.[25,26] It is reported that QD-based LFA provides ten times more sensitivity than the commonly used gold nanoparticle-based LFA.[27] Moreover, several emerging strategies including quantum yield (QY) enhancement and QD loading on nanocarriers have been developed to further improve the sensitivity of QD-based LFA.[28] Loading quantum dots (QDs) onto the surface of nanocarriers, such as SiO_2 nanoparticles or polystyrene nanobeads, results in the formation of quantum nanobeads (QBs). This process, which can be achieved through methods like polyethyleneimine (PEI)-mediated electrostatic adsorption, enhances the luminescent properties of QBs, thereby improving the sensitivity of LFA devices.[29–31] Wang *et al.* introduced a QB-based LFA for SARS-CoV-2 antigen detection with the limit of detection (LOD) of 5 pg mL^{-1}.[29] QB-based LFAs hold great potential as a platform for tear biomarker analysis for glaucoma screening.

In this study, we developed a QB-based LFA for the quantitative and simultaneous detection of BDNF and TNF-α in tear fluid. The PEI-mediated electrostatic adsorption method was used to generate a 2-layer SiO_2-core QD-shell nanocomposite. After conjugating with detective antibodies for BDNF and TNF-α, the QB-antibody conjugates were loaded at the conjugate pad (Fig. 1a). To simultaneously detect the BDNF and TNF-α, the paired capture anti-BDNF antibody and capture anti-TNF-α antibody were printed at certain areas at the membrane as the test lines (Fig. 1a). Goat anti-mouse IgG which is species-specific for the detective antibodies was dispensed as control line to validate the test. Captured QBs were excited by selected light. The assembled LFA strip was placed in a cassette and inserted into the dark box, which was 3D printed and integrated with LED light and bandpass filter for image capturing (Fig. 1b). The fluorescence images were captured *via* smartphone camera and the intensity was analyzed by ImageJ. As far as we are

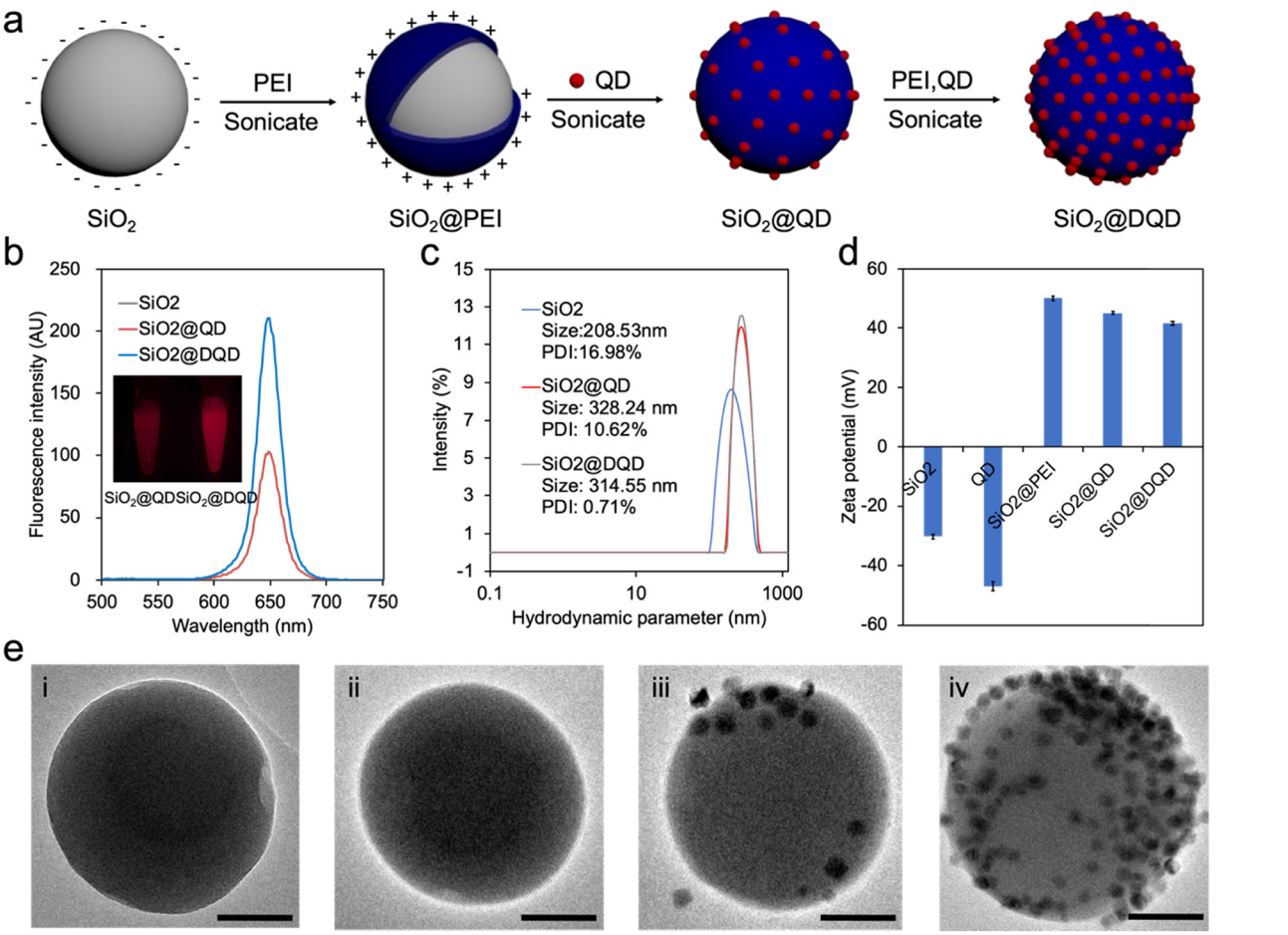

Fig. 2 Fabrication and characterization of QB. a. The schematic illustration of fabrication process of QB. The SiO_2 is treated with PEI to form a positively charged layer. Subsequently, the QDs will self-adsorb onto the surface of the SiO_2@PEI. By repeating the PEI coating and QD adsorption process, a double-layered QB is obtained. b. The fluorescence intensity of SiO_2, SiO_2@QD and SiO_2@DQD. The inset in (b) displays the photographs of the SiO_2@QD and SiO_2@DQD solution under blue light. c. The hydrodynamic size of SiO_2, SiO_2@QD and SiO_2@DQD. d. The zeta potential of SiO_2, QD, SiO_2@PEI, SiO_2@QD and SiO_2@DQD. e. The fluorescence intensity of SiO_2, SiO_2@QD and SiO_2@DQD. e The TEM images of (i) SiO_2, (ii) SiO_2@PEI, (iii) SiO_2@QD and (iv) SiO_2@DQD. Scale bars represent 50 nm.

aware, until now, no dual-target LFA has been developed for tear biomarkers in glaucoma. This study introduces a promising method for glaucoma detection by analyzing BDNF and TNF-α *via* a QB-based dual-test LFA. The limit of detection (LOD) for detection of BDNF and TNF-α reached to 4.13 and 3.39 pg mL^{-1}, respectively. The selectivity, accuracy and stability were all demonstrated, making it a promising tool for POC glaucoma screening. By providing a powerful alternative for the quantitative analysis of tear fluid biomarkers, this QB-based LFA addresses a critical need in glaucoma detection, potentially improving early diagnosis and treatment outcomes for patients worldwide.

Results and discussion

Fabrication and characterization of double-layer QBs

Attaching quantum dots to the surface of a nanocarrier can improve the luminescent capacities of the label, significantly enhancing the sensitivity of the LFA.[32] SiO_2 is widely used as a nanocarrier due to its easily decorated properties and high stability.[28] As demonstrated in Fig. 2a, to fabricate double-layer QBs, a layer-by-layer assembly strategy *via* PEI-mediated electrostatic adsorption of QDs onto the surface of SiO_2 sphere was used. After treatment with branched PEI under sonication, multiple positive charges self-assemble on the surface of the negatively charged SiO_2. This allows multiple negatively charged QDs to effectively attach to the surface, forming a stable nanoparticle with higher luminescence compared with a single QD.[29–31,33] Moreover, the addition of a second layer of the QD shell onto the SiO_2@QD are prepared as SiO_2@DQD to further improve the loading of QDs and fluorescence intensity.[29–31,33]

The fluorescent properties of the QB were characterized using a microplate reader. The SiO_2 alone showed no fluorescence signal, while the fluorescence intensity of SiO_2@DQD was approximately twice that of SiO_2@QD (Fig. 2b). This increase is attributed to the fact that the amount of QD attached in SiO_2@DQD is double that attached in SiO_2@QD. The absolute quantum yield of SiO_2@DQD was measured at 27.66%. These strong fluorescence properties of SiO_2@DQD ensure their practical use in the LFA strips. As shown in Fig. 2c, the hydrodynamic diameter of SiO_2, SiO_2@QD and SiO_2@DQD were 208.53, 328.24 and 314.55 nm respectively, indicating the successful absorption of QDs onto SiO_2. The zeta potential significantly increased after the PEI assembly and decreased with QD adsorption (Fig. 2d), consistent with the theory that the synthesis of SiO_2@DQD was driven by the electrostatic adsorption of positively charged PEI. The morphology and structure of the SiO_2@DQD was characterized by transmission electron microscopy (TEM) (Fig. 2e). Fig. 2ei–iv displays the high-resolution TEM images of SiO_2, SiO_2@QD and SiO_2@DQD respectively. The SiO_2 is particles have an average diameter of around 180 nm and exhibit a spherical morphology with a smooth surface (Fig. 2ei). A transparent PEI layer with a thickness of 2 nm was observed, supporting the successful coating of PEI onto the SiO_2 surface (Fig. 2eii). With the successive double adsorption of the QDs, the number of QDs on the SiO_2@DQD surface is significantly higher than that on the SiO_2@QD surface (Fig. 2eiii and iv).

Optimization of the QB-based LFA strip

The carboxyl group functionalized QDs were employed in this study. Double layers of QDs provided sufficient carboxyl groups and an enlarged surface for antibody conjugation. The 1-ethyl-3-(3-dimethylamino propyl)-carbodiimide (EDC) and *N*-hydroxysulfosuccinimide sodium salt (NHS) mediated coupling strategy was used to form a stable conjugate of QB and anti-TNF-α antibody. The carboxyl groups are activated by EDC and interacted with the amino groups of the antibodies (Fig. 3a). The average hydrodynamic diameter of QBs and QB-antibody conjugates were 288.23 mm and 361.60 nm (Fig. 3b). The zeta potential value decreased from +41.52 mV for the QBs to +36.82 mV for the QB-antibody conjugates (Fig. 3c). These results indicate the successful attachment of antibody molecules onto the surfaces of the QBs. The TEM image demonstrated a 5 mm gray layer surrounding the QB, representing the antibody conjugated with the QBs (Fig. 3d).

A LFA strip typically consists of a sample pad, a conjugate pad, a reaction membrane, and an absorbance pad. The conjugate pad is crucial because the analyte in the sample interacts with the labeled detective antibody on the conjugate pad before the mixture moves to the membrane. Therefore, pre-treatment of the conjugate pad is essential to maintain antibodies stability and functionality, ensuring the consistent and uniform release of analyte-antibody mixtures.[34] Bovine serum albumin (BSA), sucrose, and Tween 20 are 3 major components of the treatment buffer.[35] BSA reduces non-specific binding between QB-antibody conjugate and the pad.[35] During the drying process sucrose coats the surface of the conjugate, preserving its bio-functionaliyt.[35] Tween 20, a common detergent, aids with the release of the conjugate from the pad.[35] Aggregation of the conjugates is another significant concern, and it has been reported that a higher concentration of Tween 20, such as 5%, can reduce aggregation through the formation of micelles around the conjugates.[36] To further characterize the effect of Tween 20, the conjugate was treated with PBS buffer containing Tween 20 concentrations of 0, 5, 10 to 15% (v/v). As shown in Fig. 3e, most of the conjugate remained on the conjugate pad when treated with buffer without Tween 20. A concentration of 10% of Tween 20 provided a brighter control line. The signal at the control line decreased when the Tween 20 concentration reached 15% (Fig. 3e). This is because a high concentration of detergent can inhibit the conjugate from adhering to the antibody.

The shape of the test and control lines play an important role in improving the accuracy of the result analysis. In this study, a liquid-dispensing instrument, Linomat 5, was used to evenly print the lines. The volume loaded in a specific area affects the performance of the LFA strip so the optimal

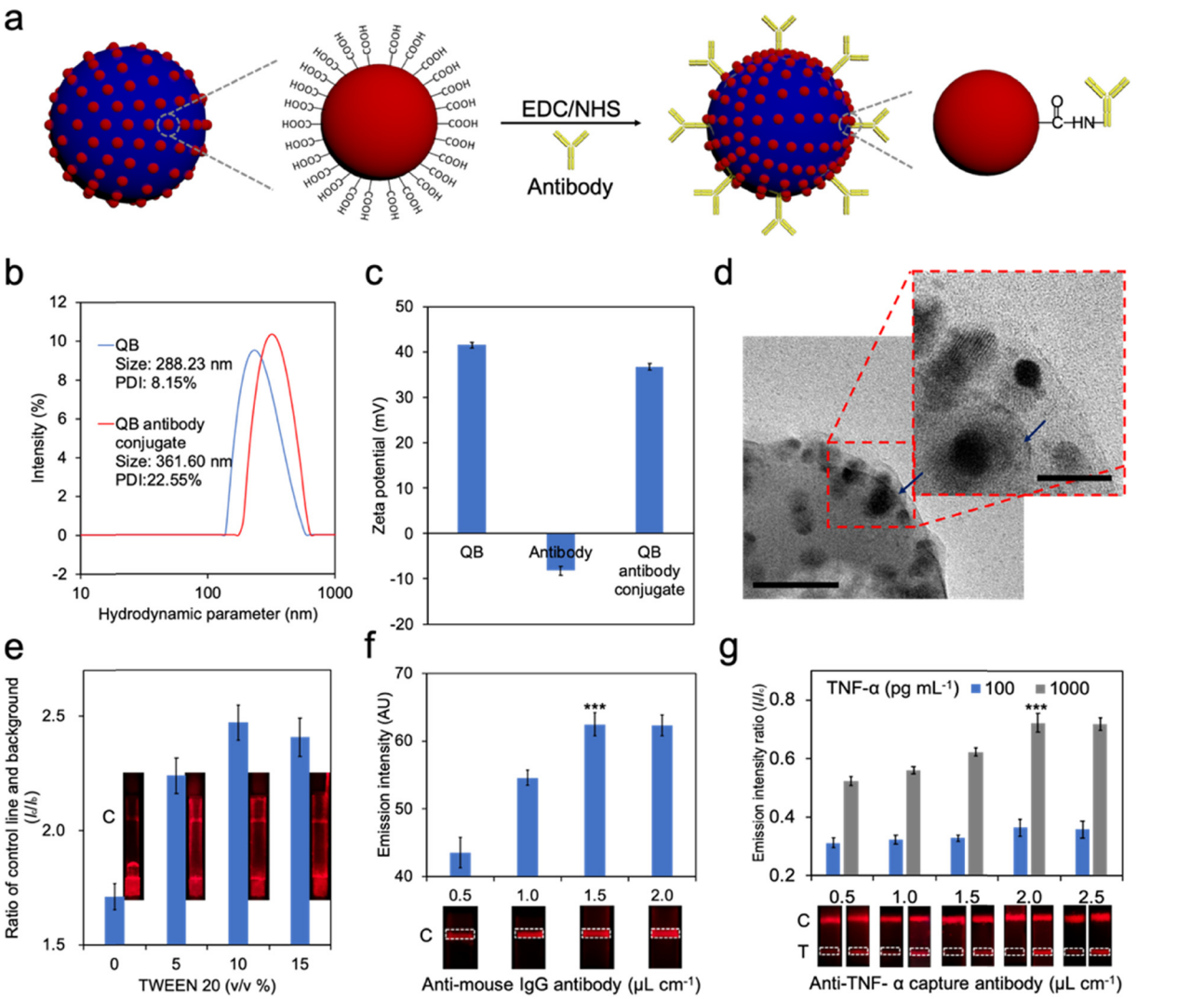

Fig. 3 Fabrication of QB-antibody conjugate and optimization of LFA strip. a. Schematic illustrating the fabrication of QB–anti-TNF-α detective antibody conjugate by EDC/NHS strategy. b. Hydrodynamic diameter of QB and QB-detective anti-TNF-α antibody conjugate. c. Zeta potential of QB and QB-detective anti-TNF-α antibody conjugate. d. The TEM images QB-detective anti-TNF-α antibody conjugate. Scale bars represent 50 nm and 20 nm. e. Optimization test of Tween 20% in the pre-treatment buffer of conjugate pad. f. Fluorescence intensity of the control line when printed different volume of anti-mouse IgG antibody. g. Ratio of emission intensity of the test line to the control line when printed different volume of anti-TNF-α capture antibody. Differences in the ratio were compared using one-way ANOVA, $P < 0.05$ was considered as statistically significant (3 strips for each group, $^{***}P < 0.001$).

volumes for the test line and control line were investigated. Anti-mouse-IgG antibody solution at a concentration of 2 mg mL^{-1} was printed as the control line with dispense volumes of 0.5, 1.0, 1.5, 2.0 μL cm^{-1}. After loading the running buffer, the fluorescence signal of the control line was analyzed. The ideal line width is between 0.8 to 1 mm,[37] therefore the analysis area was 3 mm by 8 mm (the grey box in Fig. 3f and g). As it shown in Fig. 3f, a higher volume of solution increased the width of the line. Additionally, a higher volume of antibody solution enhanced signal strength due to the increased quantity of antibodies, leading to greater capture of the QB-antibody–analyte mixture. It was evident that loading 1.5 μL cm^{-1} anti-mouse-IgG antibody solution provided higher fluorescence intensity and formed an evenly distributed line. For the test line, the anti-TNF-α capture antibody solution should be dispensed in 2 μL cm^{-1} (Fig. 3g).

Performance of the single test LFA strip

A single test TNF-α LFA strip was firstly developed under optimal conditions. The performance of the lateral flow assay (LFA) strip in quantitatively measuring TNF-α was firsted evaluated by introducing samples containing varying concentrations of TNF-α. When excited by the blue light, two distinct visible red fluorescence bands become apparent: a test line and a control line. When the concentration of TNF-α increased from 0 to 400 pg mL^{-1}, the fluorescence intensity of the test line exhibited a corresponding increase, and the signal from the control line remained unchanged (Fig. 4a).

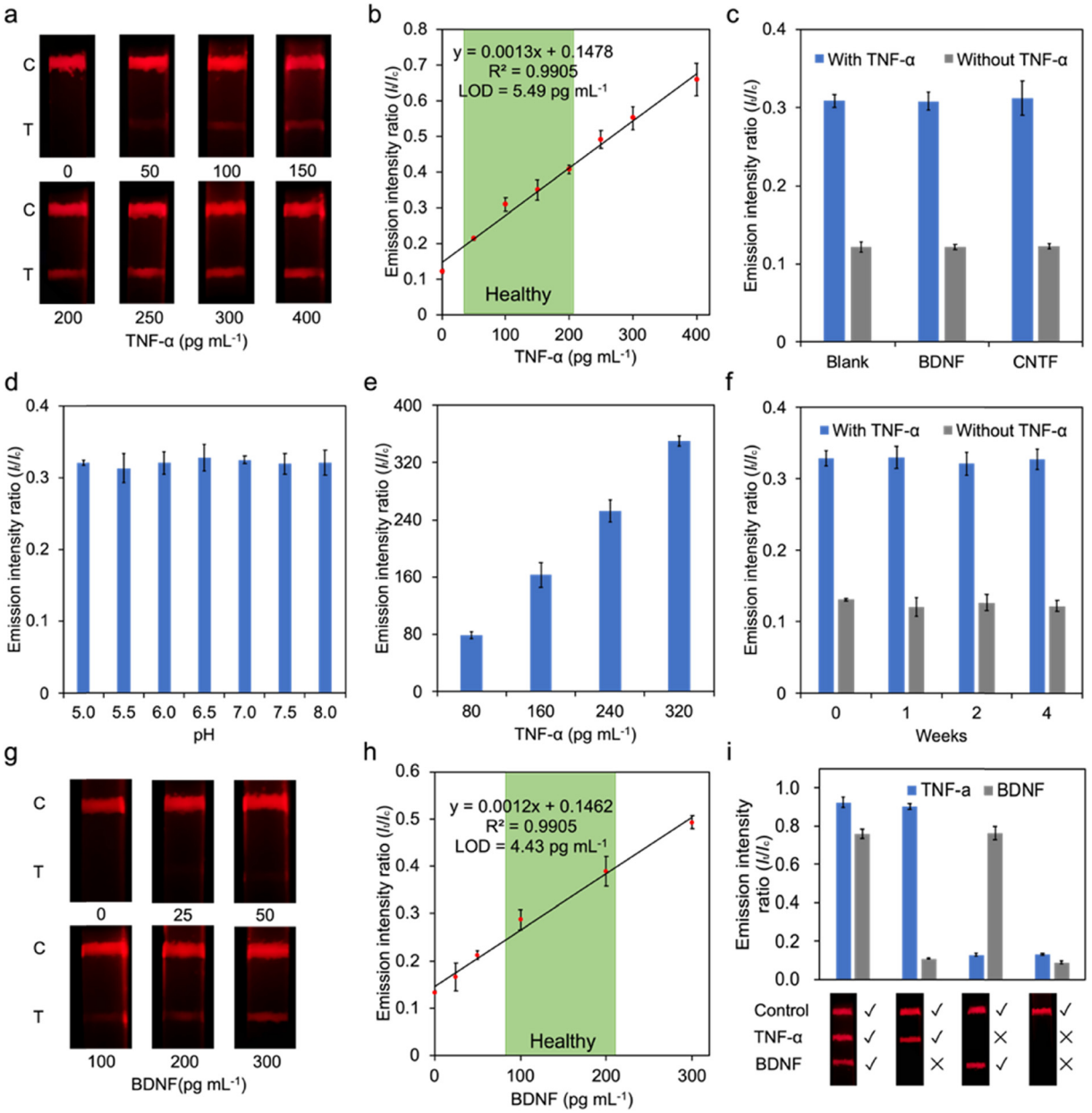

Fig. 4 TNF-α and BDNF detection in artificial tear fluid using single-test LFA strip. a. Fluorescence images of the strips before and after loading artificial tear fluid samples with varying concentrations of TNF-α. b. The linear relationship between emission intensity ratio of teat line to control line (I_t/I_c) and TNF-α concentration. c. The emission intensity ratio (I_t/I_c) after loading artificial tear fluid contains different proteins, including BDNF (200 pg mL^{-1}) and CNTF (60 pg mL^{-1}), with or without TNF-α (100 pg mL^{-1}). d. The emission intensity ratio (I_t/I_c) after loading artificial tear fluid sample with 100 pg mL^{-1} TNF-α concentration at different pH values. e. The recovery test in artificial tear fluid with concentrations of 80, 160, 240 and 320 pg mL^{-1}. f. The emission intensity ratio (I_t/I_c) after loading the artificial tear fluid sample with TNF-α concentrate in 100 pg mL^{-1} to strips stored in the lab environment for 0, 1, 2, and 4 weeks in the dark, respectively. g. The fluorescence images of the reading area of the strips before and after loading artificial tear fluid samples with different volumes of BDNF. h. The linear relationship between the emission intensity ratio and concentration of BDNF. i. The emission intensity ratio after loading artificial tear fluid samples containing different components: both TNF-α (100 pg mL^{-1}) and BDNF (100 pg mL^{-1}), TNF-α (100 pg mL^{-1}) only, BDNF (100 pg mL^{-1}) only and neither.

The fluorescence intensity of test lines and control lines were quantified through ImageJ, and the intensity ratio of test and control lines (I_t/I_c) was calculated. Consequently, a standard curve was created to demonstrate the relationship between I_t/I_c and TNF-α levels ranging from 0 to 400 pg mL^{-1} (Fig. 4b). This range covers the health range of TNF-α (110.7 ± 87.2 pg mL^{-1})[38] and can distigusih between glaucoma patients and healthy patients, who typically have increased TNF-α level in their tear fluid.[18] The R^2 value was 0.9902, and the detection limit (LOD) was determined to be 5.49 pg mL^{-1} using the international union of pure and appl. chem. (IUPAC) protocol (LOD = y_{blank} + 3 SD_{blank}).

A selectivity test was performed to exclude the effect of well-studied glaucoma biomarkers: BDNF[12] and CNTF.[39] As

shown in Fig. 4c, the presence of BDNF or CNTF within the artificial tear fluid samples does not yield positive results. Moreover, when loading artificial tear fluid samples containing both BDNF and TNF-α, or CNTF and TNF-α, the I_t/I_c values were similar to those of samples only containing only TNF-α (Fig. 4c). The remarkable selectivity of this strip to TNF-α indicates the high specificity of these antibodies, making it suitable for the development of multiplex test LFAs.

The effect of pH was also considered, as the pH of tears ranges from 6.5 to 7.6,[40] and be more acidic in certain disorders or due to medication usage, such as in glaucoma.[41,42] Artificial tear fluid samples containing 100 pg mL^{-1} CNTF with a pH range from 5.0 to 8.0 were prepared to assess the stability of the TNF-α LFA strip under different pH conditions. The results showed minimal differences between different groups (Fig. 4d), indicating the negligible effect of pH. The accuracy of this LFA strip were assessed using artificial tear fluid samples spiked with different concentrations of TNF-α (80, 160, 240 and 320 pg mL^{-1}). The measured level of TNF-α in these samples were 78.85, 163.02, 252.81 and 350.11 pg mL^{-1}, with recoveries ranging from 98.56% to 109.41% (Fig. 4e). These results demonstrate the high accuracy of the strip in detecting TNF-α. The performance of this LFA was also evaluated after being stored for 1 to 4 weeks under room temperature in opaque aluminum foil pouches with desiccants. Even after a month of storage, the I_t/I_c values remain consistent with those obtained using freshly fabricated strip (Fig. 4f).

A single test strip for BDNF detection was then developed following the same setting as the aforementioned TNF-α LFA. Brighter test lines were observed after loading artificial samples with higher levels of BDNF (Fig. 4g), and a standard curve with an LOD 4.43 pg mL^{-1} was established (Fig. 4h). To further develop the dual-test LFA for the simultaneous detection of TNF-α and BDNF, it was essential to verify the absence of cross-reactivity between TNF-α and BDNF, as well as their respective antibody pairs. Artificial tear fluid samples were prepared to contain both TNF-α and BDNF, TNF-α only, BDNF only, or neither of them. Anti-TNF-α detective antibody and anti-BDNF detective antibody were printed separately to the membrane, forming two distinct test lines. The prepared samples were then tested by this dual-test LFA. As shown in Fig. 4i, the TNF-α and BDNF groups exhibited distinct signal bands on their corresponding test lines, while the negative control sample demonstrated no perceivable fluorescence

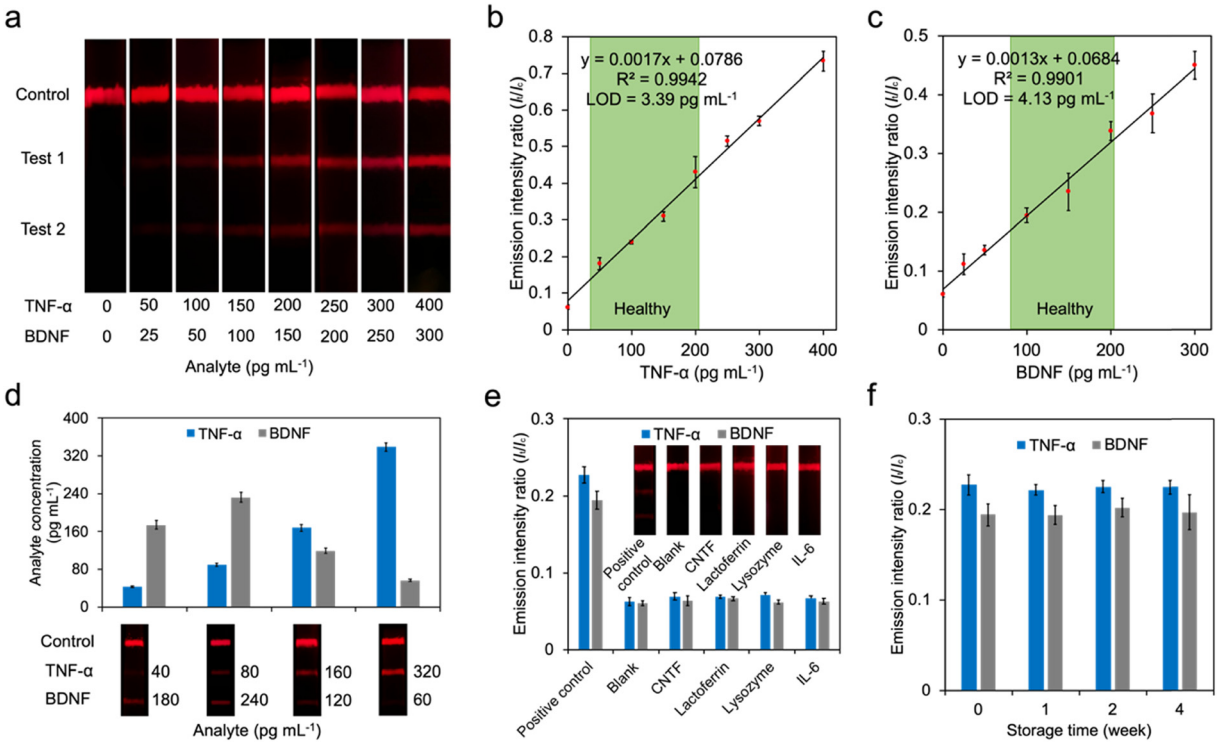

Fig. 5 Fabrication and characterization of dual-test LFA strip for simultaneous quantitation of BDNF and TNF-α. a. The fluorescence images of the dual-test strips before and after loading artificial tear fluid samples with varying concentrations of BDNF and TNF-α. b. The linear relationship between emission intensity ratio and concentration of TNF-α. c. The linear relationship between emission intensity ratio and concentration of BDNF. d. Recovery results for BDNF and TNF-α spiked in artificial tear fluid samples. e. The emission intensity ratio after loading artificial tear fluid contains different proteins, including positive control TNF-α (100 pg mL^{-1}) and BDNF (100 pg mL^{-1}), negative control (no extra protein), CNTF (60 pg mL^{-1}), lactoferrin (2.2 mg mL^{-1}) and IL-6 (30 pg mL^{-1}). f. The emission intensity ratio after loading artificial tear fluid sample with TNF-α concentrate in 100 pg mL^{-1} and BDNF concentrate in 100 pg mL^{-1} to strips stored in the lab environment for 0, 1, 2, and 4 weeks in the dark, respectively.

Table 1 Recovery results for BDNF and TNF-α spiked in artificial tear fluid samples

Condition	Added level (pg mL^{-1})	Detected level (pg mL^{-1})	Recovery	CV[a] (%)
Sample 1 (glaucoma)	BDNF: 60	57.05	95.08%	7.81
	TNF-α: 320	338.98	105.93%	4.42
Sample 2 (normal)	BDNF: 120	120.58	100.48%	8.91
	TNF-α: 160	169.55	105.97%	8.89
Sample 3 (smoker)	BDNF: 240	232.12	96.72%	7.81
	TNF-α: 80	90.01	112.51%	7.03
Sample 4	BDNF: 180	174.41	96.89%	8.47
	TNF-α: 40	42.81	107.01%	6.22

[a] CV: coefficient of variation (n = 3).

signal. These results demonstrate minimal cross-reactivity between TNF-α and BDNF, and a strong ability to distinguish these two biomarkers in tear samples.

Dual-test LFA strip for simultaneously detection of TNF-α and BDNF

To increase the sensitivity and specificity of our test, we created a dual LFA capable of concurrently assessing TNF-α and BDNF, which exhibit opposing trends in disease progression of glaucoma. The feasibility of this dual-test LFA strip for simultaneous and quantitative detection of TNF-α and BDNF was verified by varying concentration of TNF-α (0–400 pg mL^{-1}) and BDNF (0–300 pg mL^{-1}). There are two major strategies for multiplexing LFA: positioning test lines spatially separately on a single strip and arranging multiple strips in an array format.[43] Although the second approach reduces the risk of reciprocal interference between assays, it significantly increases the costs of fabrication and sample volume required. Moreover, the limited cross-reactivity between our target analytes and their antibodies also meets the requirements for fabricating the dual-test LFA in the first format. Therefore, a LFA strips with two test lines and one control line was fabricated. As shown in Fig. 5a, the fluorescence intensity of both test lines 1 and 2 gradually increased with higher levels of TNF-α and BDNF. Similar with the single-test LFA, two standard curves were constructed by plotting I_t/I_c against concentrations of TNF-α and BDNF with the R^2 values 0.9942 and 0.9901, respectively. The LODs for TNF-α and BDNF were 3.39 pg mL^{-1} and 4.13 pg mL^{-1}, comparable with commercial ELISA kits with LODs of 4.32 pg mL^{-1} and 2.40 pg mL^{-1} (Table 2).

To evaluate the practical applications of this dual-test LFA strip, the assay was then conducted to detect TNF-α and BDNF spiked in artificial tear fluid samples. For instance, sample 1 was spiked with 320 pg mL^{-1} TNF-α and 60 pg mL^{-1} BDNF to simulate tears from patients with primary open-angle glaucoma (POAG). For those tears collected from people without POAG, 160 pg mL^{-1} TNF-α and 120 pg mL^{-1} BDNF were spiked. As shown in Fig. 5d and demonstrated in Table 1, the average recoveries of the LFA strip ranged from 95.08% to 112.51% for TNF-α and from 105.93% to 107.01% for BDNF. These results demonstrate the high accuracy of this dual-test LFA for the simultaneous quantification of two biomarkers. The coefficient of variations (CV) for both TNF-α and BDNF were calculated, ranging from 4.42% to 8.91%, well within the acceptable limit (less than 10%), indicating excellent reproducibility (Table 1).

To further characterize the practical application, the selectivity of the dual-test LFA to other interfering substances involved in glaucomatous processes including CNTF,[51] lactoferrin,[52] lysozyme[53] and IL-6 (ref. 17) was also investigated. As shown in Fig. 5e, two fluorescence bands were observed when loading artificial tear samples containing 100 pg mL^{-1} TNF-α and 100 pg mL^{-1} BDNF, whereas samples contain CNTF, lactoferrin, lysozyme and IL-6 exhibited extremely low perceivable fluorescence signaling on the test lines. These results demonstrated high specificity

Table 2 Comparison of methods for TNF-α and BDNF detection

Analyte	Detection methods	Label	Body fluid	LOD	Ref.
TNF-α	Multi-test LFA	Up conversion nanoparticles	Gingival crevicular fluid	4.439 ng mL^{-1}	44
	Dual-test LFA	Fluorescent microspheres	Plasma	10.7 pg mL^{-1}	45
	Electrochemical impedance spectroscopy	—	Human serum	1 pg mL^{-1}	46
	Electrochemical immunosensor	Carbon dot	Human serum	0.05 pg mL^{-1}	47
	ELISA	Enzyme	—	4.32 pg mL^{-1}	—
	LFA	QB	Artificial tear	3.39 pg mL^{-1}	This work
BDNF	Biolayer interferometry	3D aptasensor	Human serum	0.2 ng mL^{-1}	48
	Electrochemical EndoChip	Gold film	Human blood	0.2 ng mL^{-1}	49
	LFA	Gold nanoparticle	Artificial tear	14.12 pg mL^{-1}	50
	ELISA	Enzyme	—	2.4 pg mL^{-1}	—
	LFA	QB	Artificial tear	4.13 pg mL^{-1}	This work

to TNF-α and BDNF. To assess the storage stability of this dual LFA, the prepared LFA strips were sealed in an aluminum foil bag containing a desiccant and stored at room temperature. After 1, 2 and 4 weeks, artificial tear fluid samples contain 100 pg mL^{-1} TNF-α and 100 pg mL^{-1} BDNF were loaded and I_t/I_c values were obtained. The consistent I_t/I_c values indicate outstanding stability after 4 weeks of storage (Fig. 5f). The relatively low storage requirements demonstrate that this LFA strip is suitable to be used in POC settings and could significantly reduce the cost of transportation.

In POC diagnostics, multiplex testing offers significant advantages by providing comprehensive diagnostic information. This is particularly important because the progression of complex diseases, such as glaucoma, is difficult to accurately assessed by measuring a single biomarker. As a result, there is a growing need for technologies capable of detecting multiple biomarkers simultaneously. In recent years, several technologies have emerged to address this need. One prominent example is protein microarrays, or protein chips.[54,55] These platforms immobilize antibodies, enzymes, or other probes on a solid carrier, such as plastic or glass, enabling the capture of specific analytes.[54,55] Over the past decade, protein microarrays have evolved to quantify dozens, or even hundreds, of analytes simultaneously, making them powerful tools for multiplex testing. Another well-established technology is the Luminex xMAP bead-based system.[56,57] This approach attaches antibodies, ligands, or nucleic acids specific to the target analytes onto fluorescence beads,[56,57] allowing the detection of up to 500 different analytes in a single test.[57] Several companies now offer customizable assays, allowing clients to add specific probes for tailored detection needs.

While both microarrays and Luminex technology exhibit remarkable sensitivity, specificity, and high throughput, they also come with certain limitations. These technologies require expensive equipment and skilled personnel to perform the tests and analyze the results, which limits their accessibility—particularly in POC settings.[58] Additionally, the high costs associated with array fabrication and reagents further restrict their use in routine diagnostics.[58] The development of multiplex LFA combines the strengths of traditional LFA, such as ease of use, portability, low cost, and rapid response, with the advantages of multiplex testing.[43] Recently, many studies have focused on developing multiplex LFA for disease diagnostics. For instance, Ekman *et al.* developed a dual-test LFA based on upconverting nanoparticles, capable of measuring the cancer-specific CA125-STn-glycosylation and CA15-3-STn-glycosylation in ascites fluid.[59] Another study analyzed the cost-effectiveness of a multiplex LFA for diagnosing enteric fever and dengue in Cambodia and Bangladesh, demonstrating that this technology is highly effective and cost-saving in low- and middle-income regions.[60] These examples underscore that multiplex LFA can meet the cost-effectiveness requirements for glaucoma screening, particularly in POC settings.

In this study, we introduce a dual-test LFA, which represents a pioneering approach by simultaneously detecting biomarkers TNF-α and BDNF, with a specific focus on glaucoma detection. Compared to individual biomarker detection tests, this dual-test LFA not only increases throughput, reduces sample and reagent requirements, and shortens analysis time but also significantly improves the accuracy of glaucoma detection. The SiO_2@DQD label, with its core-dual shell nanostructure containing numerous QDs, enhances the performance of the dual-test LFA, achieving superior sensitivity with LODs of 3.39 pg mL^{-1} for TNF-α and 4.13 pg mL^{-1} for BDNF. These LOD values are notably lower than the physiological range of TNF-α (approximately 100 pg mL^{-1} in healthy individuals, with higher levels in patients) and BDNF (78.0 ± 25.1 pg mL^{-1} in patients compared to 116.2 ± 43.1 pg mL^{-1} in healthy controls), allowing for clear differentiation between patients and healthy individuals. These LOD values are also lower than those reported for most paper-based detection platforms, including our previous work (Table 2). The high-performing antibodies for TNF-α and BDNF provide the dual-test LFA with exceptional selectivity, high accuracy with recovery ranging from 95.08% to 112.51%, as well as excellent reproducibility. Overall, the performance of this dual-test LFA is comparable to the gold standard protein detection method, ELISA but without requiring costly instruments or well-trained technicians, making this dual-test LFA particularly suitable for POC settings (Table S2†).

Quantitative analysis of fluorescence signals is a crucial factor in achieving accurate biomarker measurement in LFA. Several research groups have utilized commercial strip readers, such as the FIC-S1 fluorescent strip reader,[61] for fluorescence signal detection[29,32,61] (Table S3†). However, these commercial devices often suffer from several limitations, including high cost, lack of portability, and the need for specialized equipment and maintenance. Some groups have developed portable readout devices. For instance, a previously reported system consisted of a handheld readout device wirelessly connected to a smartphone for quantitative result analysis[62] (Table S3†). This system uses an optical detection module on a stepping motor to scan the test strip, with photodiodes capturing the fluorescence signal before transmission to smartphone *via* Wi-Fi or Bluetooth.[62] While this improves portability, the multi-step signal conversion—from optical detection to electrical signals and then wireless transmission—may introduce signal loss, reducing accuracy. Additionally, reliance on Wi-Fi or Bluetooth can limit usability in resource-limited settings. We adopted a different approach by employing a 3D-printed readout box, where fluorescence signals were directly captured using a smartphone camera. Modern smartphones are equipped with high-resolution cameras, ensuring accurate fluorescence imaging with minimal signal loss. Our results also demonstrated the

excellent performance of smartphone-based analysis methods.

This study introduces an innovative approach to glaucoma monitoring by analyzing TNF-α and BDNF levels in tears using a QB-based LFA system. This dual-test LFA is ideal for meeting the demand for sensitive, rapid, and quantitative measurement of TNF-α and BDNF levels in tears within POC settings.

Conclusion

In this work, a QB-based dual-test LFA strip was developed for the highly sensitive and simultaneous quantitative detection of TNF-α and BDNF levels in tear fluid. The innovative QB labels were fabricated *via* PEI-mediated layer-by-layer electrostatic adsorption, resulting in hundreds of QDs covering the surface of a SiO_2 core. Consequently, this dual-test LFA exhibits outstanding detection capability, with LOD of 3.39 pg mL^{-1} for TNF-α and 4.13 pg mL^{-1} for BDNF. The LFA also demonstrated excellent accuracy and reproducibility. The minimal cross-reactivity observed with other factors associated with glaucoma pathogenesis in tear fluid indicates a high degree of selectivity, comparable to commercially available standard methods. Furthermore, the smartphone-assisted readout system proved to be user-friendly and cost-effective, making it well-suited for point-of-care diagnostics and screening.

This QB-based LFA demonstrates significant potential as a robust platform for tear fluid analysis. The LODs of this LFA are low, surpassing the minimal physiological concentrations of TNF-α and BDNF, ensuring accurate measurement even within the lower ranges of these biomarkers' physical presence. Additionally, the QB-based LFA can simultaneously measures two different biomarkers, significantly enhancing the efficiency and speed of the test. This multiplex capability conserves valuable tear samples, which are often available in limited quantities, and reduces the likelihood of false results, thereby improving overall test accuracy.

This platform has great potential for expansion to detect multiple biomarkers on a single strip, further enhancing its sensitivity and specificity. The implementation of an automated smartphone reading application, will enable the test to become more accessible and user-friendly, even outside clinical environments. Further clinical trials are needed to validate the performance of this dual-test LFA. Standardized tear collection methods, such as Schirmer strips or microcapillary tubes, will be implemented to obtain a fixed tear volume, followed by appropriate dilution strategies to ensure consistency across samples and enhance the assay's robustness and reliability in clinical applications. Overall, the developed dual-test LFA presents an optimal solution for timely, cost-effective, and precise glaucoma screening in POC settings. This proposed method not only holds significant promise for glaucoma detection but also possesses considerable market potential.

Materials and methods

Materials and instruments

Albumin, bovine serum albumin, calcium chloride, glucose, magnesium chloride, phosphate-buffered saline, potassium chloride, sucrose, tween 20, sodium chloride, lysozyme, lactoferrin, tris-hydrochloride, tris base, *N*-(3-dimethylaminopropyl)-*N*′-ethylcarbodiimide hydrochloride (EDC), *N*-hydroxysulfosuccinimide sodium salt (NHS) and carboxylic group functionalized CdSe/ZnS core–shell quantum dots were obtained from Sigma-Aldrich. All components of the lateral flow test strip, including the backing, sample pad, conjugate pad, react membrane (FF170HP), and absorbent pad, were obtained from Whatman.

The absorbance spectrum was measured through a microplate reader (Varioskan LUX Multimode, ThermoFisher). The quantum dots, SiO_2, quantum beads were characterized by the microplate reader, high-resolution transmission electron microscope (TEM) (JEOL STEM/TEM 2100Plus), and Litesizer (Anton Paar). The QD-antibody was purified with the centrifuge (Thermo Scientific). The test line and control line were dispensed by a liquid dispense system (CAMAG® Linomat 5). The readout box was produced by the 3D printer (UltiMaker S7 Pro Bundle). The images were captured by iPhone X.

Fabrication of quantum bead

SiO_2 based high intensity QB was fabricated *via* PEI-based electrostatic self-assembly strategy. First, 16 μL of SiO_2 was added into the 40 mL of aqueous PEI solution and sonicated for 50 min. Then, the resulting SiO_2@PEI spheres were washed with DDI water by centrifugation (6000 rpm, 8 min) three times under room temperature to remove unreacted PEI. The SiO_2@PEI were redispersed in 4 mL of DDI water and mixed with 16 μL of QDs solution for 60 min stirring. The QDs rapidly self-assembled onto the surface of the positively charged SiO_2@PEI to form SiO_2@QD. The obtaining SiO_2@QD were centrifuged (5000 rpm, 6 min) at room temperature and dissolved in 4 mL of DDI water. The PEI coating and QD adhering process was repeat again to generate SiO_2@DQD. Finally, the prepared SiO_2@DQD were collected by centrifugation (5000 rpm, 6 min) and stored in 4 mL of ethanol for future use.

QBs and antibody conjugation

The QBs and detective antibody conjugate were prepared through the EDC/NHS strategy. 1 mL of prepared SiO_2@DQD was centrifuged and resuspended in a tube with 500 μL MES solution (0.1 M, pH 5.5). 5 μL of fresh EDC (0.1 M) solution and 10 μL of fresh NHS (0.1 M) solution were added and reaction for 5 min. The activated SiO_2@DQDs were centrifuged (5000 rpm, 6 min) and resuspended in 0.2 mL of PBS solution (pH 7.4, containing 0.05% Tween 20). Subsequently, 40 μL of detective anti-TNF-α antibody (0.5 mg

mL^{-1}) was added into the mixture and incubated for 2 hours at room temperature. Next, 100 μL of 10% BSA was added to block any unreacted carboxyl sites of Si@DQD antibody conjugate. Finally, the mixture was centrifuged at 5000 rpm at room temperature for 6 min, and the precipitate was suspended in 200 μL of PBS solution containing 1% BSA.

Preparation of the LFA strip

The LFA strip consisted of sample pad, conjugate pad, membrane and absorbance pad. The sample pad treated with PBS buffer containing tween 20 (1% v/v) and BSA (1% w/v). The conjugate pad was pre-treated with the conjugate pad buffer containing different volume of tween 20, BSA (1% w/v) and sucrose (5% w/v). 10 μL QB–anti-BDNF antibody conjugate and QB–anti-TNF-α antibody mixture solution was loaded into the conjugate pad. The detective anti-BDNF antibodies and detective anti-TNF-α antibodies were dispensed into membrane in test line 1 and test line 2 using a dispensor. The donkey anti-mouse IgG antibodies were loaded at the control line in the membrane. All parts of the LFA strips were assembled at a backing with a 2 mm overlap finally.

Image captured and data analysis

The image capture box and LFA case were made by 3D printing. The images were captured by iPhone X camera. Then the images were converted into 8-bit black/white by ImageJ. ImageJ obtained the grey values of selected bands representing their fluorescence intensity.

The LOD was calculated using eqn (1).

$$\text{LOD} = \text{Mean of blank data} + 3 \times (\text{Standard deviation of blank data}) \quad (1)$$

The coefficient of variation (CV%) was calculated using eqn (2).

$$\text{CV\%} = \text{Standard deviation/Mean} \quad (2)$$

The results were shown as I_t/I_c. Each group contained at least three strips.

Data availability

The data that support the findings of this study are available from the corresponding author upon reasonable request.

Conflicts of interest

The authors declare no competing financial interests regarding the work described in this manuscript.

References

1 M. Shi, Y. Tian, Y. Luo, T. Elze and M. Wang, RNFLT2Vec: Artifact-corrected representation learning for retinal nerve fiber layer thickness maps, *Med. Image Anal.*, 2024, **94**, 103110.
2 X. R. Gao, F. Wu, P. T. Yuhas, R. K. Rasel and M. Chiariglione, Automated vertical cup-to-disc ratio determination from fundus images for glaucoma detection, *Sci. Rep.*, 2024, **14**(1), 4494.
3 N. Y. Q. Tan, D. S. Friedman, I. Stalmans, I. I. K. Ahmed and C. C. A. Sng, Glaucoma screening: where are we and where do we need to go?, *Curr. Opin. Ophthalmol.*, 2020, **31**(2), 91–100.
4 V. Shih, M. Parekh, J. K. Multani, C. B. McGuiness, C.-C. Chen, J. H. Campbell, E. Miller-Ellis and M. M. G. Olivier, Clinical and Economic Burden of Glaucoma by Disease Severity: A United States Claims-Based Analysis, *Ophthalmol., Glaucoma*, 2021, **4**(5), 490–503.
5 R. Chou, S. Selph, I. Blazina, C. Bougatsos, R. Jungbauer, R. Fu, S. Grusing, D. E. Jonas and S. Tehrani, Screening for Glaucoma in Adults: Updated Evidence Report and Systematic Review for the US Preventive Services Task Force, *JAMA, J. Am. Med. Assoc.*, 2022, **327**(20), 1998–2012.
6 S. Hamid, P. Desai, P. Hysi, J. M. Burr and A. P. Khawaja, Population screening for glaucoma in UK: current recommendations and future directions, *Eye*, 2022, **36**(3), 504–509.
7 W. H. Swanson, B. J. King, M. S. Alluwimi and R. Malik, Predicting perimetric defects from en face maps of retinal nerve fibre layer reflectance, *Ophthalmic Physiol. Opt.*, 2024, 613–625.
8 C. Wada-Koike, R. Terauchi, K. Fukai, K. Sano, E. Nishijima, K. Komatsu, K. Ito, T. Kato, M. Tatemichi, Y. Kabata and T. Nakano, Comparative Evaluation of Fundus Image Interpretation Accuracy in Glaucoma Screening Among Different Physician Groups, *Clin. Ophthalmol.*, 2024, **18**, 583–589.
9 S. Hagan, E. Martin and A. Enríquez-de-Salamanca, Tear fluid biomarkers in ocular and systemic disease: potential use for predictive, preventive and personalised medicine, *EPMA J.*, 2016, **7**(1), 15.
10 A. Osborne, T. Z. Khatib, L. Songra, A. C. Barber, K. Hall, G. Y. X. Kong, P. S. Widdowson and K. R. Martin, Neuroprotection of retinal ganglion cells by a novel gene therapy construct that achieves sustained enhancement of brain-derived neurotrophic factor/tropomyosin-related kinase receptor-B signaling, *Cell Death Dis.*, 2018, **9**(10), 1007.
11 M. Almasieh, A. M. Wilson, B. Morquette, J. L. Cueva Vargas and A. Di Polo, The molecular basis of retinal ganglion cell death in glaucoma, *Prog. Retinal Eye Res.*, 2012, **31**(2), 152–181.
12 A. A. Shpak, A. B. Guekht, T. A. Druzhkova, K. I. Kozlova and N. V. Gulyaeva, Brain-Derived Neurotrophic Factor in Patients with Primary Open-Angle Glaucoma and Age-related Cataract, *Curr. Eye Res.*, 2018, **43**(2), 224–231.
13 A. A. Kondkar, T. Sultan, F. A. Almobarak, H. Kalantan, S. A. Al-Obeidan and K. K. Abu-Amero, Association of increased levels of plasma tumor necrosis factor alpha with primary open-angle glaucoma, *Clin. Ophthalmol.*, 2018, **12**, 701–706.

14 R. Agarwal and P. Agarwal, Glaucomatous neurodegeneration: an eye on tumor necrosis factor-alpha, *Indian J. Ophthalmol.*, 2012, **60**(4), 255–261.
15 G. Tezel, TNF-alpha signaling in glaucomatous neurodegeneration, *Prog. Brain Res.*, 2008, **173**, 409–421.
16 B. Burgos-Blasco, B. Vidal-Villegas, F. Saenz-Frances, L. Morales-Fernandez, L. Perucho-Gonzalez, J. Garcia-Feijoo and J. M. Martinez-de-la-Casa, Tear and aqueous humour cytokine profile in primary open-angle glaucoma, *Acta Ophthalmol.*, 2020, **98**(6), e768–e772.
17 J. Benitez-Del-Castillo, J. Cantu-Dibildox, S. M. Sanz-Gonzalez, V. Zanon-Moreno and M. D. Pinazo-Duran, Cytokine expression in tears of patients with glaucoma or dry eye disease: A prospective, observational cohort study, *Eur. J. Ophthalmol*, 2019, **29**(4), 437–443.
18 J. M. Martinez-de-la-Casa, F. Perez-Bartolome, E. Urcelay, J. L. Santiago, J. Moreno-Montañes, P. Arriola-Villalobos, J. M. Benitez-Del-Castillo and J. Garcia-Feijoo, Tear cytokine profile of glaucoma patients treated with preservative-free or preserved latanoprost, *Ocul. Surf.*, 2017, **15**(4), 723–729.
19 S. Balaiya, J. Edwards, T. Tillis, V. Khetpal and K. V. Chalam, Tumor necrosis factor-alpha (TNF-α) levels in aqueous humor of primary open angle glaucoma, *Clin. Ophthalmol.*, 2011, **5**, 553–556.
20 A. Civera, P. Galan-Malo, I. Segura-Gil, L. Mata, A. P. Tobajas, L. Sánchez and M. D. Pérez, Development of sandwich ELISA and lateral flow immunoassay to detect almond in processed food, *Food Chem.*, 2022, **371**, 131338.
21 S. Marquez, J. Liu and E. Morales-Narváez, Paper-based analytical devices in environmental applications and their integration with portable technologies, *Curr. Opin. Environ. Sci. Health*, 2019, **10**, 1–8.
22 R. Gupta, P. Gupta, S. Wang, A. Melnykov, Q. Jiang, A. Seth, Z. Wang, J. J. Morrissey, I. George, S. Gandra, P. Sinha, G. A. Storch, B. A. Parikh, G. M. Genin and S. Singamaneni, Ultrasensitive lateral-flow assays via plasmonically active antibody-conjugated fluorescent nanoparticles, *Nat. Biomed. Eng.*, 2023, **7**(12), 1556–1570.
23 A. Gonzalez, M. Gaines, L. Y. Gallegos, R. Guevara and F. A. Gomez, Thread- paper, and fabric enzyme-linked immunosorbent assays (ELISA), *Methods*, 2018, **146**, 58–65.
24 J. D. Bishop, H. V. Hsieh, D. J. Gasperino and B. H. Weigl, Sensitivity enhancement in lateral flow assays: a systems perspective, *Lab Chip*, 2019, **19**(15), 2486–2499.
25 A. Foubert, N. V. Beloglazova and S. De Saeger, Comparative study of colloidal gold and quantum dots as labels for multiplex screening tests for multi-mycotoxin detection, *Anal. Chim. Acta*, 2017, **955**, 48–57.
26 M. Hu, X. Hu, G. Wang, Y. Cheng, X. Yu, X. Huang and Y. Li, A fluorescent lateral flow immunoassay based on CdSe/CdS/ZnS quantum dots for sensitive detection of olaquindox in feedstuff, *Food Chem.*, 2023, **419**, 136025.
27 R. Wu, S. Zhou, T. Chen, J. Li, H. Shen, Y. Chai and L. S. Li, Quantitative and rapid detection of C-reactive protein using quantum dot-based lateral flow test strip, *Anal. Chim. Acta*, 2018, **1008**, 1–7.
28 B. Fang, Q. Xiong, H. Duan, Y. Xiong and W. Lai, Tailored quantum dots for enhancing sensing performance of lateral flow immunoassay, *TrAC, Trends Anal. Chem.*, 2022, **157**, 116754.
29 C. Wang, X. Yang, S. Zheng, X. Cheng, R. Xiao, Q. Li, W. Wang, X. Liu and S. Wang, Development of an ultrasensitive fluorescent immunochromatographic assay based on multilayer quantum dot nanobead for simultaneous detection of SARS-CoV-2 antigen and influenza A virus, *Sens. Actuators, B*, 2021, **345**, 130372.
30 X. Cheng, S. Zheng, W. Wang, H. Han, X. Yang, W. Shen, C. Wang and S. Wang, Synthesis of two-dimensional graphene oxide-fluorescent nanoprobe for ultrasensitive and multiplex immunochromatographic detection of respiratory bacteria, *Chem. Eng. J.*, 2021, **426**, 131836.
31 C. Li, Z. Zou, H. Liu, Y. Jin, G. Li, C. Yuan, Z. Xiao and M. Jin, Synthesis of polystyrene-based fluorescent quantum dots nanolabel and its performance in H5N1 virus and SARS-CoV-2 antibody sensing, *Talanta*, 2021, **225**, 122064.
32 X. Yang, Q. Yu, X. Cheng, H. Wei, X. Zhang, Z. Rong, C. Wang and S. Wang, Introduction of Multilayered Dual-Signal Nanotags into a Colorimetric-Fluorescent Coenhanced Immunochromatographic Assay for Ultrasensitive and Flexible Monitoring of SARS-CoV-2, *ACS Appl. Mater. Interfaces*, 2023, **15**(9), 12327–12338.
33 S. Zheng, X. Yang, B. Zhang, S. Cheng, H. Han, Q. Jin, C. Wang and R. Xiao, Sensitive detection of Escherichia coli O157:H7 and Salmonella typhimurium in food samples using two-channel fluorescence lateral flow assay with liquid Si@quantum dot, *Food Chem.*, 2021, **363**, 130400.
34 M. Kaur and E. Eltzov, Optimizing Effective Parameters to Enhance the Sensitivity of Vertical Flow Assay for Detection of Escherichia coli, *Biosensors*, 2022, **12**(2), 63.
35 Y. Wu, Y. Hu, N. Jiang, R. Anantharanjit, A. K. Yetisen and M. F. Cordeiro, Quantitative brain-derived neurotrophic factor lateral flow assay for point-of-care detection of glaucoma, *Lab Chip*, 2022, **22**(18), 3521–3532.
36 J. G. Bruno, Advantages and Disadvantages of Using Quantum Dots in Lateral Flow and Other Biological Assay Formats. in *Application of Quantum Dots in Biology and Medicine: Recent Advances*, ed. P. Barik and S. Mondal, Springer Nature Singapore, Singapore, 2022, pp. 91–102.
37 M. A. Nash, J. M. Hoffman, D. Y. Stevens, A. S. Hoffman, P. S. Stayton and P. Yager, Laboratory-scale protein striping system for patterning biomolecules onto paper-based immunochromatographic test strips, *Lab Chip*, 2010, **10**(17), 2279–2282.
38 S. S. Çomoğlu, H. Güven, M. Acar, G. Öztürk and B. Koçer, Tear levels of tumor necrosis factor-alpha in patients with Parkinson's disease, *Neurosci. Lett.*, 2013, **553**, 63–67.
39 A. A. Shpak, A. B. Guekht, T. A. Druzhkova, K. I. Kozlova and N. V. Gulyaeva, Ciliary neurotrophic factor in patients with primary open-angle glaucoma and age-related cataract, *Mol. Vision*, 2017, **23**, 799–809.
40 M. B. Abelson, I. J. Udell and J. H. Weston, Normal human tear pH by direct measurement, *Arch. Ophthalmol.*, 1981, **99**(2), 301.

41 M. S. Norn, Tear fluid pH in normals, contact lens wearers, and pathological cases, *Acta Ophthalmol.*, 1988, **66**(5), 485–489.
42 Y. Azuamah, A. Ugwuoke, G. Ogbonna, N. Ikoro, E. Esenwah and A. Megwas, International Journal of Research Effect of Topical 1% Pilocarpine on the Ocular Tear Film pH, *Int. J. Res.*, 2019, **06**, 120–128.
43 L. Anfossi, F. Di Nardo, S. Cavalera, C. Giovannoli and C. Baggiani, Multiplex Lateral Flow Immunoassay: An Overview of Strategies towards High-throughput Point-of-Need Testing, *Biosensors*, 2018, **9**(1), 2.
44 W. He, M. You, Z. Li, L. Cao, F. Xu, F. Li and A. Li, Upconversion nanoparticles-based lateral flow immunoassay for point-of-care diagnosis of periodontitis, *Sens. Actuators, B*, 2021, **334**, 129673.
45 G. J. Worsley, S. L. Attree, J. E. Noble and A. M. Horgan, Rapid duplex immunoassay for wound biomarkers at the point-of-care, *Biosens. Bioelectron.*, 2012, **34**(1), 215–220.
46 P. Kongsuphol, H. H. Ng, J. P. Pursey, S. K. Arya, C. C. Wong, E. Stulz and M. K. Park, EIS-based biosensor for ultra-sensitive detection of TNF-alpha from non-diluted human serum, *Biosens. Bioelectron.*, 2014, **61**, 274–279.
47 S. Sri, G. Lakshmi, P. Gulati, D. Chauhan, A. Thakkar and P. R. Solanki, Simple and facile carbon dots based electrochemical biosensor for TNF-alpha targeting in cancer patient's sample, *Anal. Chim. Acta*, 2021, **1182**, 338909.
48 S. Gao, Q. Li, S. Zhang, X. Sun, X. Zheng, H. Qian and J. Wu, One-step high-throughput detection of low-abundance biomarker BDNF using a biolayer interferometry-based 3D aptasensor, *Biosens. Bioelectron.*, 2022, **215**, 114566.
49 M. Bockaj, B. Fung, M. Tsoulis, W. G. Foster and L. Soleymani, Method for Electrochemical Detection of Brain Derived Neurotrophic Factor (BDNF) in Plasma, *Anal. Chem.*, 2018, **90**(14), 8561–8566.
50 Y. Wu, Y. Hu, N. Jiang, R. Anantharanjit, A. K. Yetisen and M. F. Cordeiro, Quantitative brain-derived neurotrophic factor lateral flow assay for point-of-care detection of glaucoma, *Lab Chip*, 2022, **22**(18), 3521–3532.
51 A. A. Shpak, A. B. Guekht, T. A. Druzhkova, K. I. Kozlova and N. V. Gulyaeva, Ciliary neurotrophic factor in patients with primary open-angle glaucoma and age-related cataract, *Mol. Vision*, 2017, **23**, 799–809.
52 D. Pieragostino, M. D'Alessandro, M. di Ioia, C. Di Ilio, P. Sacchetta and P. Del Boccio, Unraveling the molecular repertoire of tears as a source of biomarkers: Beyond ocular diseases, *Proteom. - Clin. Appl.*, 2015, **9**(1–2), 169–186.
53 D. Pieragostino, L. Agnifili, V. Fasanella, S. D'Aguanno, R. Mastropasqua, C. Di Ilio, P. Sacchetta, A. Urbani and P. Del Boccio, Shotgun proteomics reveals specific modulated protein patterns in tears of patients with primary open angle glaucoma naïve to therapy, *Mol. BioSyst.*, 2013, **9**(6), 1108–1116.
54 G. Chen, L. Yang, G. Liu, Y. Zhu, F. Yang, X. Dong, F. Xu, F. Zhu, C. Cao, D. Zhong, S. Li, H. Zhang and B. Li, Research progress in protein microarrays: Focussing on cancer research, *Proteom. - Clin. Appl.*, 2023, **17**(1), 2200036.
55 Y. Xia, H. Chen, J. Li, H. Hu, Q. Qian, R.-X. He, Z. Ding and S.-S. Guo, Acoustic Droplet-Assisted Superhydrophilic–Superhydrophobic Microarray Platform for High-Throughput Screening of Patient-Derived Tumor Spheroids, *ACS Appl. Mater. Interfaces*, 2021, **13**(20), 23489–23501.
56 W. Rountree, H. E. Lynch, T. N. Denny, G. D. Sempowski and A. N. Macintyre, Sources of variability in Luminex bead-based cytokine assays: Evidence from twelve years of multi-site proficiency testing, *J. Immunol. Methods*, 2024, **531**, 113699.
57 A. H. Ren, E. P. Diamandis and V. Kulasingam, Uncovering the Depths of the Human Proteome: Antibody-based Technologies for Ultrasensitive Multiplexed Protein Detection and Quantification, *Mol. Cell. Proteomics*, 2021, **20**, 100155.
58 B. Zhang, G. B. Salieb-Beugelaar, M. M. Nigo, M. Weidmann and P. Hunziker, Diagnosing dengue virus infection: rapid tests and the role of micro/nanotechnologies, *Nanomed.: Nanotechnol., Biol. Med.*, 2015, **11**(7), 1745–1761.
59 M. Ekman, T. Salminen, K. Raiko, T. Soukka, K. Gidwani and I. Martiskainen, Spectrally separated dual-label upconversion luminescence lateral flow assay for cancer-specific STn-glycosylation in CA125 and CA15-3, *Anal. Bioanal. Chem.*, 2024, **416**(13), 3251–3260.
60 R. Chew, C. Painter, W. Pan-Ngum, N. P. J. Day and Y. Lubell, Cost-effectiveness analysis of a multiplex lateral flow rapid diagnostic test for acute non-malarial febrile illness in rural Cambodia and Bangladesh, *Lancet Reg. Health - Southeast Asia The*, 2024, **23**, 100389.
61 X. Yang, X. Liu, B. Gu, H. Liu, R. Xiao, C. Wang and S. Wang, Quantitative and simultaneous detection of two inflammation biomarkers via a fluorescent lateral flow immunoassay using dual-color SiO(2)@QD nanotags, *Microchim. Acta*, 2020, **187**(10), 570.
62 Y. Wang, H. Chen, H. Wei, Z. Rong and S. Wang, Tetra-primer ARMS-PCR combined with dual-color fluorescent lateral flow assay for the discrimination of SARS-CoV-2 and its mutations with a handheld wireless reader, *Lab Chip*, 2022, **22**(8), 1531–1541.